

# A New Spatial Block-Correlation Model for Fluid Antenna Systems

Pablo Ramírez-Espinosa, David Morales-Jimenez, and Kai-Kit Wong

**Abstract**—Powered by position-flexible antennas, the emerging fluid antenna system (FAS) technology postulates as a key enabler for massive connectivity in 6G networks. The free movement of antenna elements within a given aperture allows several users to share the same radio channel at no additional cost and without the need of precoding. However, the true potential of FAS is still unknown due to the high spatial correlation of the wireless channel between very close-by antenna positions, which yields intractable analyses for conventional correlation models such as Jake’s. Therefore, there is an outstanding need for simple yet accurate correlation models that allow to unveil the multiplexing capabilities of FAS, since realistic classical models are prohibitively complex while state-of-the-art approximations may be too simplistic. Aiming to fill this gap, we here propose a general framework to approximate spatial correlation by block-diagonal matrices, motivated by the well-known block fading assumption and by statistical results on large correlation matrices. The proposed block-correlation model makes the performance analysis possible, and tightly approximates the results obtained with realistic models such as Jake’s and Clarke’s. We finally leverage our framework to characterize slow-fluid antenna multiple access (slow-FAMA) systems, evaluating their performance for both one- and two-dimensional fluid antennas.

## I. INTRODUCTION

Fluid antenna system (FAS) is an emerging and very promising technology, focused on dynamic antenna architectures, which is recently attracting a very substantial interest as a key enabler for multiple access in upcoming 6G systems [1]. Conceptually, FAS encapsulates any system in which the antenna elements can be moved within a predefined aperture, either virtually or physically. This includes all forms of position-flexible antennas such as on-off switching pixels [2, 3], liquid-based radiating structures [4], or movable antenna systems as recently proposed in [5]; see these works and the references therein for more details on physical implementations.

This work is supported in part by the State Research Agency (AEI) of Spain under grant PID2020-118139RB-I0/AEI/10.13039/501100011033. The work of P. Ramírez-Espinosa is supported by a “María Zambrano” Fellowship funded by the European Union – Next Generation EU via the Ministry of Universities of the Spanish Government. The work of D. Morales-Jimenez is supported by AEI and the European Social Fund under grant RYC2020-030536-I. The work of K. K. Wong is supported by the Engineering and Physical Sciences Research Council (EPSRC) under Grant EP/W026813/1.

P. Ramírez-Espinosa and D. Morales-Jimenez are with Dept. Signal Theory, Networking and Communications, Universidad de Granada, Granada 18071, Spain (e-mail: pre@ugr.es, dmorales@ugr.es).

K.-K. Wong is with the Department of Electronic and Electrical Engineering, University College London, London WC1E 6BT, U.K. (e-mail: kai-kit.wong@ucl.ac.uk). He is also affiliated with Yonsei Frontier Laboratory, Yonsei University, Seoul, 03722, Korea.

This work has been submitted to the IEEE for publication. Copyright may be transferred without notice, after which this version may no longer be accessible.

The key idea behind FAS is similar to that in classical diversity systems with fixed antennas, i.e., exploiting the spatial diversity to minimize interference or maximize the received signal strength. However, in contrast to conventional arrays, the *antennas* in FAS—more rigorously, *radiating elements*, since not all the physical implementations involve the use of conventional antennas—can be freely moved within the available aperture. Ideally, the space (continuum) can be “sampled” at any arbitrary point, providing additional degrees of freedom, although in practice only a finite (albeit dense) mesh of sampling points may be available.

Based on the dynamic capabilities of FAS (i.e., how fast the radiating elements can be moved either virtually or physically), two multiple access solutions have been proposed: *i*) fast-fluid antenna multiple access (FAMA), where the system switches on a symbol-by-symbol basis [6, 7]; and *ii*) slow-FAMA, where the switching is carried out at every channel time-coherence interval [8]. While the former is deemed impractical due to implementation limitations, the latter arises as a more feasible and realistic solution.

Although FAS was originally envisioned as one-dimensional systems, i.e., the radiating elements can be moved along a line, the same concept can be extended to 2D structures. In fact, preliminary results in [9] suggest that the degrees of freedom provided by FAS may be ramped up when extended to planar apertures. That is, instead of sampling the received signal along a line, we seek for the most convenient point (e.g., lowest interference) within a 2D surface. Despite their promising potential, 2D FAS is still at a very early research stage, and further studies are required both in terms of physical realizations and theoretical analysis (modeling and performance).

Regardless whether we look at one- or two-dimensional FAS, a key limitation is that the channel in the space continuum is *inherently correlated*. Having (infinitely) many switchable antenna ports (pixels, or switching positions) packed, adjacent to one another, unavoidably increases the correlation between these positions. A well-known fundamental fact is that, to sample “independent” channels, antennas should be placed at a minimum distance of  $\lambda/2$ ; a theoretical result that arises from spatial correlation in isotropic propagation environments [10, 11]. This minimum distance could be seen as the “spatial sampling rate” to exploit the channel’s spatial diversity, raising the fundamental question: *what is the benefit of the “oversampling” in FAS?* Besides, the larger the number of ports for a given aperture—spatial points where the received signal can be sampled—the higher the correlation between them. This renders diminishing returns and, ultimately, leads

to a saturation effect as shown in [6, 12]. Hence, *how much do we need to oversample to obtain the full potential of FAS?* These two questions, despite being essential, remain still open.

Naturally, to properly address the previous questions and to theoretically assess the performance of FAS, appropriate channel correlation models need to be considered. Thus far, most of the works dealing with FAS adopt Jake’s correlation model (e.g., [6–9, 11–17]), which arises from a 2D isotropic propagation where all the scatterers are uniformly distributed in a ring around the receiver [18]. However, the analysis of FAS under Jake’s model is prohibitively complex. Substantial efforts have been made to come up with simplified, yet accurate correlation models, aimed to serve as good approximations while allowing for a tractable analysis [6, 8, 12, 13]. An approximation to Jake’s correlation—based on using only a few dominant eigenvalues of the resulting correlation matrix—is proposed in [6, 12], resulting in intricate expressions requiring computing as many integrals as ports available in the FAS. A simpler model (analysis is possible) was introduced in [13], where Jake’s correlation is replaced by a “constant” correlation parameter such that pairs of ports are equally correlated, rendering a correlation matrix with equal entries. Despite having been assumed since early FAS contributions [8, 19–23], its validity to realistically (accurately) model the spatial correlation between close-by radiating elements is questioned.

Aiming to retain the analytical tractability of the “constant” correlation model in [13], while accurately modeling (approximating) a realistic scenario, we here propose an alternative method to characterize the correlation inherent to FAS. Inspired by the coherence interval idea behind block-fading models, we consider that the spatial correlation remains approximately constant within a block (set of ports), while being independent between blocks. This resembles the concept of time coherence interval in Jake’s channel autocorrelation model. Based on this *spatial coherence interval*, the key idea is approximating a given spatial correlation matrix (e.g., Jake’s) with a block-diagonal matrix by means of spectral analysis. Statistical theory for large Toeplitz matrices (by extension, correlation matrices) dictates that, as the number of ports increases for a given aperture, the matrix tends to be dominated by a small fraction of eigenvalues (as noted in [6, 12]). Hence, each of the blocks can “capture” one of the eigenvalues, yielding a block-diagonal matrix with similar spectrum to that of the target correlation matrix. This approximation framework enables a tractable analysis of FAS and paves the way towards further studies on their fundamental limits. Overall, the contributions of this paper are summarized as:

- Motivated by the outstanding need of simple and yet accurate models for FAS, we propose a block-diagonal spatial correlation model that can capture the spectral characteristics of arbitrary spatial correlation functions—thus providing a trade-off solution between accuracy and mathematical tractability.
- Building upon statistical theory of large Toeplitz matrices, we present an algorithm to efficiently approximate the fluid antenna correlation structure based on the block-diagonal framework. The proposed method is particularly

simple to evaluate, in contrast to conventional correlation models (especially for 2D fluid antennas).

- The proposed solution is applied to slow-FAMA systems, yielding tractable expressions for the outage probability, as well as simple approximations and upper bounds.
- A performance evaluation of slow-FAMA is carried out, highlighting the benefit of the oversampling rendered by FAS, their multiplexing capacity, and the ability of the block-diagonal approximation to capture the different effects inherent to these systems.

The remainder of this paper is organized as follows: Section II provides an overview of spatial correlation models and presents the channel model for FAS. Section III details the proposed framework to approximate correlation in FAS. Section IV carries out the performance analysis of slow-FAMA systems based on the block-diagonal approximation. Section V presents the performance evaluation of slow-FAMA and, finally, some conclusions are drawn in Section VI.

*Notation:* Vectors and matrices are represented by bold lowercase and uppercase symbols, respectively,  $(\cdot)^T$  denotes the matrix transpose, and  $\|\cdot\|_2$  is the  $\ell_2$  norm of a vector. Also,  $(\mathbf{A})_{j,k}$  is the  $j, k$ -th element of  $\mathbf{A}$ . Finally,  $j = \sqrt{-1}$  is the imaginary number, and  $\mathbb{E}[\cdot]$  is the mathematical expectation. Any other specific notation will be defined when necessary.

## II. CHANNEL AND SPATIAL CORRELATION MODELS IN FAS

In principle, channel modeling for FAS should not be any different from conventional multi-antenna channel modeling, with one key exception: the importance of *spatial correlation*. Indeed, the high correlation between ports as a consequence of the arbitrarily close spacing means that particular attention should be paid to its characterization. Recently, the popularity of intelligent surfaces and dense arrays has brought back the interest in spatial channel correlation [10, 24], extending classical formulations such as Clarke’s and Jake’s models [18, 25, 26]. In fact, despite being the preferred choice in the FAS literature, Jake’s is not but one possible model, representing a specific propagation scenario as we shall see later. Due to the capital importance of spatial correlation in FAS, we revisit here a general channel modeling approach, and how the different assumptions on the propagation environment lead to different spatial correlation models.

### A. Spatial correlation for Rayleigh channels

Let us consider, as in [26], an antenna element at an arbitrary position  $\mathbf{r}_n = (x_n \ y_n \ z_n)^T$  in the 3D space. Assuming far-field propagation and some source (transmitter) exciting the scenario with a narrowband transmission, the complex base-band signal (channel)  $h_n$  received at  $\mathbf{r}_n$  is given by the superposition of  $P$  plane waves (paths) as

$$h_n = \sum_{p=1}^P \alpha_p G(\phi_p, \theta_p) \exp(j\mathbf{k}(\phi_p, \theta_p)^T \mathbf{r}_n), \quad (1)$$

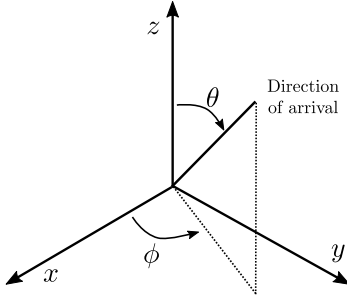


Fig. 1. Coordinates system.

where  $\alpha_p \in \mathbb{C}$  is the gain of the  $p$ -th path,  $\phi_p \in [0, 2\pi)$  and  $\theta_p \in [0, \pi)$  are the azimuth and polar arrival angles (see Fig. 1),  $G(\phi_p, \theta_p)$  is the antenna pattern, and

$$\mathbf{k}(\phi_p, \theta_p) = k (\sin \theta_p \cos \phi_p \quad \sin \theta_p \sin \phi_p \quad \cos \theta_p)^T \quad (2)$$

with  $k = 2\pi/\lambda$  the wavenumber. To further elaborate, we need to impose conditions on some of the variables in (1). A common assumption is considering that  $\alpha_p \forall p$  are independent random variables<sup>1</sup> with  $\mathbb{E}[\alpha_p] = 0$  and  $\mathbb{E}[|\alpha_p|^2] = \sigma_\alpha^2/P$ , with  $\sigma_\alpha^2 > 0$ . That is, the total received power is equally distributed between all the incoming plane-waves. Besides, unless going very high in frequency, the number of paths  $P$  is typically large, and thus the central limit theorem applies. Therefore,  $h_n$  is Gaussian distributed with moments

$$\mathbb{E}[h_n] \stackrel{(a)}{=} \sum_{p=1}^P \mathbb{E}[\alpha_p] \mathbb{E}[G(\phi_p, \theta_p) e^{j\mathbf{k}(\phi_p, \theta_p)^T \mathbf{r}_n}] = 0, \quad (3)$$

$$\mathbb{E}[|h_n|^2] \stackrel{(a)}{=} \frac{\sigma_\alpha^2}{P} \sum_{p=1}^P \mathbb{E}[|G(\phi_p, \theta_p)|^2], \quad (4)$$

where the independence between  $\alpha_p$  and  $\theta_p, \phi_p$  is assumed in (a). This twofold assumption gives rise to the so-called Rayleigh fading. The interest lies then in the relation between the channel experienced by two nearby antenna elements located at  $\mathbf{r}_n$  and  $\mathbf{r}_m$ , which due to the plane wave assumption, experience the same path gains and angles of arrival. We look hence at the cross-moment

$$\begin{aligned} \sigma_{n,m}^2 &= \mathbb{E}[h_n h_m^*] \\ &= \frac{\sigma_\alpha^2}{P} \sum_{p=1}^P \mathbb{E}[|G(\phi_p, \theta_p)|^2 \exp(j\mathbf{k}(\phi_p, \theta_p)^T (\mathbf{r}_n - \mathbf{r}_m))] \\ &\stackrel{(b)}{=} \sigma_\alpha^2 \mathbb{E}[|G(\phi, \theta)|^2 \exp(j\mathbf{k}(\phi, \theta)^T (\mathbf{r}_n - \mathbf{r}_m))], \end{aligned} \quad (5)$$

where (b) comes from assuming that, for every path, the angles of arrival are independent and equally distributed with density  $f_{\theta, \phi}(\theta, \phi)$ .

The spatial correlation for the Rayleigh channel depends therefore on *i*) the radiation pattern of the antennas, and *ii*) the distribution of the angles of arrival, which is imposed by the propagation environment. For simplicity, isotropic antennas are

<sup>1</sup>The randomness is justified by assuming that each plane wave in (1) is the result of multiple unresolvable reflections within the scatterer rendering the  $p$ -th path.

widely assumed, yielding  $|G(\phi, \theta)|^2 = 1$ . On the other hand, a tractable assumption is considering isotropic propagation, giving rise to the 3D Clarke's model [26]. In this case,  $\theta$  and  $\phi$  are independent with densities

$$f_\theta(\theta) = \frac{\sin(\theta)}{2}, \quad f_\phi(\phi) = \frac{1}{2\pi}, \quad (6)$$

which, introduced into (5), leads to [10, 24, 26]

$$\sigma_{n,m}^2 = \sigma_\alpha^2 \frac{\sin(k\|\mathbf{r}_n - \mathbf{r}_m\|_2)}{k\|\mathbf{r}_n - \mathbf{r}_m\|_2} = \sigma_\alpha^2 \text{sinc}(k\|\mathbf{r}_n - \mathbf{r}_m\|_2), \quad (7)$$

where  $\text{sinc}(z) = \frac{\sin(z)}{z}$ . Clearly, we see that  $\sigma_{n,m}^2 = 0$  for  $\|\mathbf{r}_n - \mathbf{r}_m\|_2 = \lambda/2$ , which leads to the well-known rule of thumb that half-wavelength spacing between antennas yields independent channels.

Let us now consider a two-dimensional scenario, i.e.,  $\mathbf{r}_n = (x_n \ y_n)$ , which corresponds to fixing  $\theta = \pi/2$ . Assume besides the same distribution for the azimuth angle as in 3D Clarke's model, given by  $f_\phi(\phi) = \frac{1}{2\pi}$ , which ultimately implies that all the plane waves arrive uniformly distributed in a ring around the receiver. Introducing these considerations into (6) yields now

$$\sigma_{n,m}^2 = \sigma_\alpha^2 J_0(k\|\mathbf{r}_n - \mathbf{r}_m\|_2), \quad (8)$$

where  $J_\nu(\cdot)$  is the  $\nu$ -th order Bessel function of the first kind. Note that (8) corresponds to Jake's correlation function (2D Clarke's model) [18, 27, 28].

It is important to notice, though, that these two examples characterize the channel correlation between points in space under isotropic propagation conditions. However, the spatial correlation function for arbitrary scenarios can be directly calculated by introducing the corresponding distribution for the angles of arrival and antenna radiation pattern in (5).

### B. Channel model for FAS

From a channel modeling perspective, a FAS can be seen as a collection of collocated radiating elements, representing the ports where the fluid antenna can switch into. Denoting by  $N$  the total number of ports, the channel vector from a transmitter is expressed as  $\mathbf{h} = (h_1(\mathbf{r}_1) \ \dots \ h_N(\mathbf{r}_N))$ , where the dependence with the (3D) position of the  $n$ -th port is explicitly stated. According to Rayleigh fading, as seen before,  $\mathbf{h}$  is jointly Gaussian distributed, i.e.,  $\mathbf{h} \sim \mathcal{CN}_N(\mathbf{0}, \sigma_\alpha^2 \boldsymbol{\Sigma})$ , with  $\boldsymbol{\Sigma} \in \mathbb{C}^{N \times N}$  the spatial correlation matrix. As discussed previously, the correlation matrix depends on the propagation environment, being in general described by  $(\boldsymbol{\Sigma})_{n,m} = \sigma_{n,m}^2 / \sigma_\alpha^2$ . Naturally, the structure of  $\boldsymbol{\Sigma}$  depends on the fluid antenna topology and, specifically, on the ports positions  $\mathbf{r}_1, \dots, \mathbf{r}_N$ . Thus, in a one-dimensional fluid antenna,  $\boldsymbol{\Sigma}$  has a Toeplitz structure. In the 2D case,  $\mathbf{h}$  represents the vectorized channel matrix, and hence the structure of  $\boldsymbol{\Sigma}$  is imposed by the port numbering. For instance, if the ports are numbered row-by-row, then  $\boldsymbol{\Sigma}$  is block Toeplitz. Note however that the physical structure is the same regardless of the port arrangement.

In the FAS literature, Jake's correlation is widely adopted for one-dimensional fluid antennas and, hence,  $\sigma_{n,m}^2$  is given by (8), i.e.,

$$(\boldsymbol{\Sigma})_{n,m} = J_0(k\|\mathbf{r}_n - \mathbf{r}_m\|_2), \quad (9)$$

representing isotropic propagation scenarios as validated in [18, Chapter 1]. However, note that Jake’s model is not valid for planar FAS, since it assumes a 2D propagation environment. Unfortunately, analytical characterization of FAS under this model is prohibitively complex. A twofold approximation to Jake’s correlation is proposed in [6]; the first approximation selects only the dominant eigenvalues of  $\Sigma$ , while the second one aims to approximate the resulting matrix by another one with similar distribution but more amenable to analysis. Still, the resulting analysis is intricate. A much simpler approach is presented in [13], modeling the channel at each port as a correlated version of a reference (and common) variable as in [29], i.e.,  $h_n = \sqrt{1 - \mu_n^2}x_n + \mu_n x_0$ , where  $x_n, x_0 \sim \mathcal{CN}(0, 1)$ . To minimize the number of parameters, [13] proposes to use a unique  $\mu_n = \mu \forall n$  chosen as the average correlation along the fluid antenna, giving as a result the constant-correlation matrix

$$\Sigma_{\text{avg}} = \begin{pmatrix} 1 & \mu^2 & \mu^2 & \dots & \mu^2 \\ \mu^2 & 1 & \mu^2 & \dots & \mu^2 \\ \vdots & & \ddots & & \vdots \\ \mu^2 & \dots & \mu^2 & \mu^2 & 1 \end{pmatrix}, \quad (10)$$

which considerably improves the tractability of the model yielding, e.g., relatively simple expressions for the outage probability for FAMA systems. This simplicity, though, comes at the price of a possibly poor accuracy when approximating (9), as illustrated in Fig. 2. It is observed that, for a reduced number of ports, the approximation in (10) is tight (mainly, because a low number of ports  $N$  translates into large spacing and hence low correlation), but the gap considerably increases as the fluid antenna is densified—which is precisely the objective of FAS. Thus, as  $N$  becomes large for a given aperture, the performance of FAS seems to be dominated by the high correlation coefficients between close-by ports, and conclusions drawn from the said constant-correlation model should at the very least be questioned.

Due to the recent popularity of FAS, there is an outstanding need to come up with simple yet accurate models which allow for characterizing the potential performance of these systems. On one hand, realistic models like Jake’s are too complex from an analytic viewpoint. On the other hand, tractable approximations like the constant-correlation model in [8] may lack accuracy because of their over-simplicity. Hence, correlation modeling for FAS is still an open problem that should be addressed with high priority.

The correlation models presented previously—Jake’s and Clarke’s—were originally developed to characterize the temporal autocorrelation of the channel; it is through the ergodicity assumption that they are extended to spatial correlation processes. In the time domain, the well-known block-fading approximation assumes independent temporal blocks with constant channel values (within each block), where the block length is determined by the channel coherence interval. Inspired by this, we here explore the idea of a block-correlation approximation to the channel’s spatial autocorrelation. That is, we aim to characterize the correlation in the fluid antenna by a block-diagonal matrix, where the correlation within each block

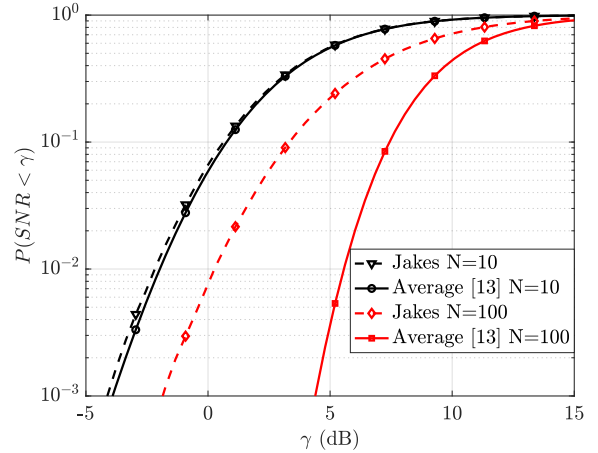


Fig. 2. Outage probability for 3 users when using a linear fluid antenna with length  $4\lambda$  when using Jake’s correlation model and the average model in [13].

is constant—as in temporal block fading—but the different blocks are independent.

### III. APPROXIMATING CORRELATION BY BLOCK-DIAGONAL MATRICES

#### A. Spectral analysis of spatial correlation matrices in FAS

The entries of the spatial correlation matrix  $\Sigma$  are obtained by “sampling” a continuous correlation function, e.g., (7) or (8), at points determined by the distance between the  $N$  ports positions. The key difference with respect to conventional antenna systems is that the number of ports is very large and, thus, the correlation function is densely sampled within the fluid antenna aperture. Leveraging sampling theory, this means we are *oversampling* the correlation function, and hence many samples are redundant and provide no extra information. Intuitively, we may think that something similar occurs with the correlation matrix  $\Sigma$  and, as  $N$  becomes large, the extra entries of  $\Sigma$  provide no additional knowledge on the spatial correlation function, leading to a rank-deficient matrix. In other words, we could expect  $\Sigma$  to be dominated by a few eigenvalues, being that more evident as  $N$  increases.

To get further insight, consider the case of a linear (one-dimensional) fluid antenna and a 3D isotropic environment such that the spatial correlation is given by (7). Denoting by  $W$  the length of the fluid antenna normalized by the wavelength, and assuming that the ports are equally spaced,  $\Sigma$  is given by the Toeplitz matrix

$$\Sigma = \begin{pmatrix} g(0) & g(1) & g(2) & \dots & g(N-1) \\ g(-1) & g(0) & g(1) & \dots & g(N-2) \\ \vdots & & \ddots & & \vdots \\ g(-N+1) & g(-N+2) & \dots & g(-1) & g(0) \end{pmatrix}, \quad (11)$$

where the generating function is

$$g(n) = \text{sinc}\left(\frac{2\pi n W}{N-1}\right). \quad (12)$$

Building upon statistical results on large Toeplitz matrices, the asymptotic properties of  $\Sigma$  are studied in the following lemma and corollary:

*Lemma 1:* Denote by  $\rho_n$  for  $n = 1, \dots, N$  the eigenvalues of  $\Sigma$  in (11), and consider the truncated Fourier series

$$f_N(x) = \sum_{n=-N/2+1}^{N/2-1} g(n)e^{jnx}, \quad x \in [-\pi, \pi]. \quad (13)$$

Then, the sequences  $\{\rho_n\}_{n=1}^N$  and  $\left\{f_N\left(\frac{2\pi(n-1)}{N}\right)\right\}_{n=1}^N$  are equally distributed in the limit  $N \rightarrow \infty$ , should  $f_N(x)$  be square-summable [30, Lemma 4.2 and Theorem 5.1].

*Corollary 1:* Consider an arbitrary small threshold  $\rho_{\text{th}}$  not larger than  $\frac{N-1}{2W}$ . Then, as  $N \rightarrow \infty$  for fixed  $W$ , the number of relevant eigenvalues of  $\Sigma$  in (11) surpassing  $\rho_{\text{th}}$  is approximated by  $2W$ .

*Proof:* From a more practical viewpoint, Lemma 1 implies that, for any continuous function  $F(x)$ ,

$$\lim_{N \rightarrow \infty} \frac{1}{N} \sum_{n=1}^N F(\rho_n) = \frac{1}{2\pi} \int_{-\pi}^{\pi} F\left(\lim_{N \rightarrow \infty} f_N(x)\right) dx. \quad (14)$$

Choosing  $F(x)$  as one approximation to the step function<sup>2</sup>, the portion of eigenvalues larger than  $\rho_{\text{th}}$  can hence be approximated by the right-hand side of (14). In the case of (11), it can be checked that the Fourier series in (13) corresponds to a rectangular wave, i.e., for large  $N$  we have

$$\begin{aligned} f_N(x) &= \sum_{n=-N/2+1}^{N/2-1} \text{sinc}\left(\frac{2\pi nW}{N-1}\right) e^{jnx} \\ &\approx \begin{cases} \frac{N-1}{2W} & \text{if } |x| \leq \frac{2\pi W}{N-1} \\ 0 & \text{otherwise} \end{cases}. \end{aligned} \quad (15)$$

Introducing the above result in (14), and using the logistic function as the step function approximation, i.e.,  $F(x) = (1 + e^{-\beta(x-\rho_{\text{th}})})^{-1}$  with  $\beta > 0$ , we readily obtain (with a slight abuse of notation)

$$\begin{aligned} \frac{1}{2\pi} \int_{-\pi}^{\pi} F\left(\lim_{N \rightarrow \infty} f_N(x)\right) dx &\approx \left(1 - \frac{2W}{N-1}\right) \frac{1}{1 + e^{\beta\rho_{\text{th}}}} \\ &+ \frac{2W}{N-1} \frac{1}{1 + e^{-\beta((N-1)/(2W)-\rho_{\text{th}})}}. \end{aligned} \quad (16)$$

The proportion of eigenvalues surpassing  $\rho_{\text{th}}$  is finally obtained by setting  $\beta$  large (so that the logistic function approximates the unitary step), leading to  $\frac{2W}{N-1}$ , and therefore the number of relevant eigenvalues is  $\frac{2W}{N-1}N \approx 2W$ . ■

Corollary 1 nicely connects with sampling theory, stating that the number of dominant eigenvalues (samples) is approximately the number of half-wavelengths contained in the fluid antenna aperture. The same analysis can be carried out for Jake's correlation (9):

*Corollary 2:* Assume a one-dimensional fluid antenna of normalized aperture  $W$ , where the spatial correlation  $\Sigma$  is given by the Toeplitz matrix generated by  $g(n) = J_0\left(\frac{2\pi nW}{N-1}\right)$  (Jake's correlation). Then, as  $N \rightarrow \infty$ , the number of eigenvalues exceeding a relatively small threshold ( $\rho_{\text{th}} < \frac{N-1}{2\pi W}$ ) is approximated by  $2W$ .

<sup>2</sup>Note that the step function itself is not a valid function since it violates the continuity assumption.

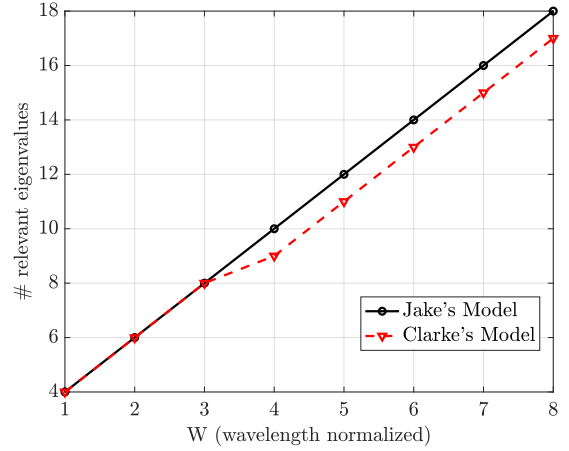


Fig. 3. Number of relevant eigenvalues in terms of the fluid antenna length. 20 ports per wavelength are considered.

*Proof:* Introducing  $g(n) = J_0\left(\frac{2\pi nW}{N-1}\right)$  into (13) and using the transform pair in [31, p. 122, Eq. (2)], we obtain that, for large  $N$ ,

$$f_N(x) \approx \begin{cases} \frac{N-1}{W\pi} \frac{1}{\sqrt{1-\left(\frac{N-1}{2\pi W}x\right)^2}} & \text{if } |x| \leq \frac{2\pi W}{N-1} \\ 0 & \text{otherwise} \end{cases}. \quad (17)$$

Using again the logistic approximation to the step function in (14), and following the same steps as in Corollary 1, the proof is completed. ■

Note that the same result stated in Corollary 2 is obtained in [6]. As an illustrative example, the number of relevant eigenvalues larger than  $N/100$ , i.e., containing 99% of the “power”, is depicted in Fig. 3, where the linear relation with  $W$  is clearly observed. Notice, however, that the number of eigenvalues is not exactly  $2W$ , due to the above result being asymptotic and the arbitrary threshold.

In the case of a 2D fluid antenna, since the resulting correlation matrix is no longer Toeplitz, the above statistical results do not directly apply. However, we may expect a similar trend, with the spatial oversampling leading to a rank-deficient correlation matrix. This is observed in Fig. 4, which plots the relevant eigenvalues (larger than 1) of a 2D fluid antenna of wavelength-normalized sizes of  $W_z \times W_x$ . Again, we see a clear linear relation between the number of dominant eigenvalues and the antenna size (in this case, its area).

Thus, building upon statistical results on large Toeplitz matrices, we have seen that both Clarke's 3D and Jake's correlation models lead to correlation matrices which, when oversampled, are dominated by a few eigenvalues (specifically, the number of half-wavelengths contained in the fluid antenna aperture). This result will be used in the next subsection to justify a block-diagonal approximation to  $\Sigma$ .

## B. Block-diagonal matrix approximation

Motivated by the tractability of the block correlation matrix in (10) [8], and the fact that  $\Sigma$  is dominated by a very few eigenvalues, we propose here a block-diagonal approximation

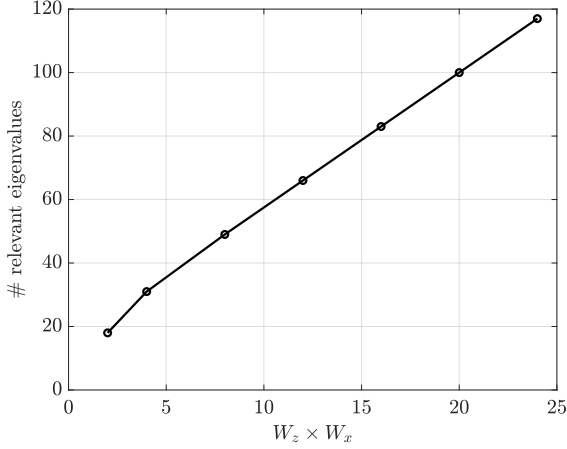


Fig. 4. Number of relevant eigenvalues in terms of the fluid antenna area. 100 ports per unit area are considered.

to the true correlation matrix with similar spectrum. That is, we seek for a matrix of the form

$$\widehat{\Sigma} \in \mathbb{R}^{N \times N} = \begin{pmatrix} \mathbf{A}_1 & \mathbf{0} & \cdots & \mathbf{0} \\ \mathbf{0} & \mathbf{A}_2 & \cdots & \mathbf{0} \\ \vdots & & \ddots & \vdots \\ \mathbf{0} & \mathbf{0} & \mathbf{0} & \mathbf{A}_B \end{pmatrix}, \quad (18)$$

where each submatrix  $\mathbf{A}_b$  is a constant correlation matrix of size  $L_b$  and correlation value  $\mu_b^2$ , i.e.,

$$\mathbf{A}_b \in \mathbb{R}^{L_b \times L_b} = \begin{pmatrix} 1 & \mu_b^2 & \cdots & \mu_b^2 \\ \mu_b^2 & 1 & \cdots & \mu_b^2 \\ \vdots & & \ddots & \vdots \\ \mu_b^2 & \cdots & \mu_b^2 & 1 \end{pmatrix}, \quad b = 1, \dots, B. \quad (19)$$

Therefore, we are interested in solving the general problem

$$\arg \min_{B, L_1, \dots, L_B, \mu_1, \dots, \mu_B} \text{dist}(\widehat{\Sigma}, \Sigma) \quad (20)$$

where  $\text{dist}(\cdot)$  is a distance metric between the approximated and true correlation matrices. Choosing the distance metric is highly non-trivial, since it is hard to predict its impact in the final application/study of interest, e.g., outage probability evaluation of slow-FAMA, where interference plays the main role. We next propose some sensible heuristic solutions.

First, notice that the form of the eigenvectors of  $\widehat{\Sigma}$  is already imposed by its block-diagonal structure, which will likely differ from the structure of the target correlation matrix  $\Sigma$ . A sensible choice is then to focus on the approximation of the spectrum (set of eigenvalues) of  $\widehat{\Sigma}$ . As shown in Appendix A, each block  $\mathbf{A}_b$  in (18) yields a set of eigenvalues  $\{\widehat{\rho}_{n'}\}_{n'=1}^{L_b}$  given by

$$\widehat{\rho}_{n'} = \begin{cases} (L_b - 1)\mu_b^2 + 1 & \text{if } n' = 1 \\ 1 - \mu_b^2 & \text{if } n' = 2, \dots, L_b \end{cases}. \quad (21)$$

Importantly, if  $\mu_b \rightarrow 1$ , then the multiple eigenvalues at  $1 - \mu_b^2$  are conveniently close to 0, and each block will produce a single dominant eigenvalue at  $(L_b - 1)\mu_b^2 + 1$ . Therefore, if we set

$\mu_b \forall b$  large, we can view each block as an approximation to a dominant eigenvalue of  $\Sigma$ . This is motivated by the previous statistical results in Corollaries 1 and 2, where the number of relevant eigenvalues of  $\Sigma$  was shown to be proportional to the number of half-wavelengths. Hence, it is reasonable to aim for one block per half-wavelength, and tune the block parameters ( $L_b$  and  $\mu_b$ ) to approximate the corresponding dominant eigenvalue. Intuitively, this choice nicely connects with the ‘‘spatial coherence interval’’ concept and the fact that channels (ports) with half-wavelength spacing should be nearly independent, and thereby represented (modeled) by independent blocks.

More specifically, consider the arbitrary small threshold  $\rho_{\text{th}}$ , and define the set of sorted eigenvalues of  $\Sigma$  larger than  $\rho_{\text{th}}$  as  $\mathcal{S}(\rho_{\text{th}}) = \{\rho_n | \rho_n > \rho_{\text{th}}, n = 1, \dots, N\}$ . Hence, we define one block in (18) per each eigenvalue in  $\mathcal{S}$ , i.e.,  $B = |\mathcal{S}|$ . Assume also, for simplicity, that  $\mu_b = \mu$  for  $b = 1, \dots, B$ , which is close to 1. As shown in the previous section,  $B \ll N$  when  $N$  becomes large. Therefore, for each  $\rho_b$  in  $\mathcal{S}$ , we select the size  $L_b$  of the corresponding block such that  $\rho_b \approx (L_b - 1)\mu^2 + 1 = \widehat{\rho}_b$ , i.e., we tune the block size to obtain a good approximation of the eigenvalue, aiming to solve

$$\arg \min_{L_1, \dots, L_B} \sum_{b=1}^B \|\rho_b - \widehat{\rho}_b\|_2. \quad (22)$$

Note that  $\sum_{b=1}^B \rho_b \approx N = \sum_{b=1}^B L_b$ ; this ensures that, ignoring rounding errors due to  $L_b$  being integer, we should be able to approximate all the eigenvalues in  $\mathcal{S}$ . The complete procedure is summarized in Algorithm 1, which iteratively increases the length of each block until either the corresponding eigenvalue is well approximated or we run out of degrees of freedom ( $\sum_b L_b = N$ ).

Regarding the choice of  $\mu$  and  $\rho_{\text{th}}$ , no closed-form solution is available. Ideally,  $\mu$  should be as close to 1 as possible, but we have empirically observed that too large values of  $\mu$  are detrimental when applying the proposed block-correlation model to FAMA analysis. Thus,  $\mu^2 \in (0.95, 0.99)$  seems to be a good rule-of-thumb. Besides, since the eigenvalues of  $\Sigma$  decay rapidly,  $\rho_{\text{th}} = 1$  usually yields accurate enough results.

As an illustrative example, Fig. 5 plots the eigenvalues of both  $\Sigma$  and  $\widehat{\Sigma}$  when the proposed method is applied to the correlation models presented in the previous section. It can be observed that the block-diagonal matrix succeeds at capturing the spectrum of the original correlation matrix. In the next sections, we evaluate how this approximation performs when used to characterize slow-FAMA systems.

### C. Independent antennas equivalent model

The proposed block-diagonal approximation aims to approximate one dominant eigenvalue of  $\Sigma$  per block, and we have seen  $\mu \rightarrow 1$  is needed to that end. Hence, a natural further approximation to the block-diagonal correlation model is directly setting  $\mu = 1$ , leading to a perfect correlation between the ports within each block. In such case, each block (regardless of its length) can be regarded (approximated) by a single antenna, and the FAS is directly approximated by a collection of  $B$  independent antennas. As shown in Corollaries

---

**Algorithm 1:** Computation of  $\widehat{\Sigma}$ 

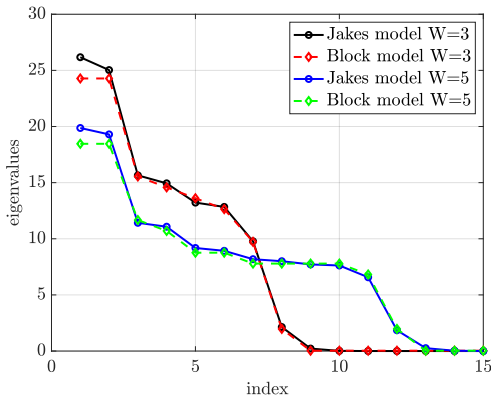

---

```

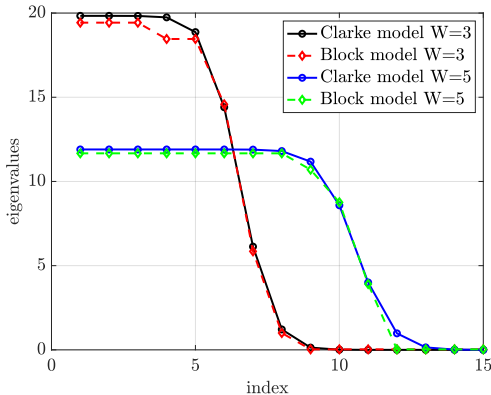
1 Input:  $S, N, \mu$ ;
2 Initialize:  $\mathcal{I} = \{1, \dots, B\}$ ,  $L_b = 0$  for  $b = 1, \dots, B$ ;
3 while  $\sum_{b=1}^B L_b < N$  do
4   foreach  $b \in \mathcal{I}$  do
5      $L_b \leftarrow L_b + 1$ ;
6     if  $|(L_b - 1)\mu^2 + 1 - \rho_b| \leq |(L_b)\mu^2 + 1 - \rho_b|$ 
7       then
8          $\mathcal{I} \leftarrow \mathcal{I} \setminus \{b\}$ ;
9     end
10  end
11 Outputs:  $\{L_1, \dots, L_B\}$ 

```

---



(a) Comparison with Jake's model



(b) Comparison with 3D Clarke's model

Fig. 5. Comparison of sorted eigenvalues for Jake's and Clarke's models and block-defined correlation matrices according to Algorithm 1. The values  $N = 120$ ,  $\mu^2 = 0.97$ , and  $\rho_{th} = 1$  have been used.

1 and 2, the number of equivalent independent antennas is related to the number of half-wavelengths contained in the aperture. This approximation can be seen as a rough—albeit extremely simple—upper bound for FAS performance, and is helpful to characterize the gain of oversampling the fluid antenna aperture.

## IV. APPLICATION TO SLOW-FAMA

### A. System Model

Consider the same system model as in [8], where a base station (BS) with several antennas simultaneously communicates with  $U$  users. The symbols intended for each user are directly transmitted from different BS antennas (without precoding) and the users are equipped with a fluid antenna of  $N$  ports (either one- or two-dimensional). Thus, in the downlink, the received signal at the  $n$ -th port of user  $u$ 's fluid antenna is

$$r_n^{(u)} = s_u h_n^{(u,u)} + \sum_{\substack{\tilde{u}=1 \\ \tilde{u} \neq u}}^U s_{\tilde{u}} h_n^{(\tilde{u},u)} + w_n^{(u)}, \quad (23)$$

where  $s_u \in \mathbb{C}$  is the symbol intended for user  $u$ ,  $h_n^{(\tilde{u},u)} \in \mathbb{C}$  is the channel gain from BS antenna dedicated for transmitting user  $\tilde{u}$ 's signal to the  $n$ -th fluid antenna port, and  $w_n^{(u)} \sim \mathcal{CN}(0, \sigma_w^2)$  is the noise term. The symbols  $s_u$  for different users are assumed to be independent with  $\mathbb{E}[s_u] = 1 \forall u$ . As detailed in Section II-B, the vector channel  $\mathbf{h}^{\tilde{u},u} = (h_1^{(\tilde{u},u)} \ h_2^{(\tilde{u},u)} \ \dots \ h_N^{(\tilde{u},u)})$  is jointly Gaussian distributed, i.e.,  $\mathbf{h}^{\tilde{u},u} \sim \mathcal{CN}_N(\mathbf{0}, \sigma_\alpha^2 \Sigma)$ .

Assuming block fading and an interference-limited scenario, within each channel coherence time, user  $u$  selects the fluid antenna port  $\hat{n}_u$  that maximizes the signal-to-interference ratio (SIR), i.e.,

$$\hat{n}_u = \arg \max_n \frac{|h_n^{(u,u)}|^2}{\sum_{\substack{\tilde{u}=1 \\ \tilde{u} \neq u}}^U |h_n^{(\tilde{u},u)}|^2}. \quad (24)$$

### B. Outage analysis

Defining by  $\gamma$  the minimum acceptable SIR for user  $u$ , we are interested in the statistical characterization of

$$P_{\text{out}}(\gamma) = P \left( \max_n \frac{|h_n^{(u,u)}|^2}{\sum_{\substack{\tilde{u}=1 \\ \tilde{u} \neq u}}^U |h_n^{(\tilde{u},u)}|^2} < \gamma \right), \quad (25)$$

which, under the correlation models in (7) and (8)—or, in general, under an arbitrary spatial correlation function given by (5)—is very complex, if not impossible [6, 9, 12, 17]. Thus, we propose approximating the outage probability by replacing the true correlation matrix  $\Sigma$  of the channel by our block-correlation matrix  $\widehat{\Sigma}$ , obtained by following Algorithm 1. That is, we assume  $\mathbf{h}^{\tilde{u},u} \sim \mathcal{CN}_N(\mathbf{0}, \sigma_\alpha^2 \widehat{\Sigma})$ . Note that this approximation is valid for both 1D and 2D fluid antennas and, in principle, for any correlation matrix beyond the examples given throughout this paper. The outage probability is therefore approximated by

$$P_{\text{out}}(\gamma) \approx \widehat{P}_{\text{out}}(\gamma) = P \left( \max_n \frac{X_n}{Y_n} < \gamma \right), \quad (26)$$

where the variables  $X_n$  and  $Y_n$  are block-wise defined as

$$X_n = \left( x_n^{(u,u)} + \frac{\mu}{\sqrt{1-\mu^2}} x_{b(n)}^{(u,u)} \right)^2 + \left( y_n^{(u,u)} + \frac{\mu}{\sqrt{1-\mu^2}} y_{b(n)}^{(u,u)} \right)^2, \quad (27)$$

$$Y_n = \sum_{\tilde{u}=1, \tilde{u} \neq u}^U \left( x_n^{(\tilde{u},u)} + \frac{\mu}{\sqrt{1-\mu^2}} x_{b(n)}^{(\tilde{u},u)} \right)^2 + \left( y_n^{(\tilde{u},u)} + \frac{\mu}{\sqrt{1-\mu^2}} y_{b(n)}^{(\tilde{u},u)} \right)^2. \quad (28)$$

All the random variables involved above—namely,  $x_j^{(u,u)}$ ,  $y_j^{(u,u)}$ ,  $x_j^{(\tilde{u},u)}$  and  $y_j^{(\tilde{u},u)}$  for  $j = n, b$ —are independent Gaussian variables with zero mean and unit variance. Besides,  $b(n)$  is the block index, i.e.,  $b(n) = 1$  for  $n = 1, \dots, L_1$ ,  $b(n) = 2$  for  $n = L_1 + 1, \dots, L_2$ , and so on. For the sake of notation, the dependence with  $n$  is dropped in the following. The resulting expression for the outage probability is hence provided in the following lemma:

*Lemma 2:* The outage probability of slow-FAMA in (25) is approximated by

$$\hat{P}_{\text{out}}(\gamma) = \prod_{b=1}^B \int_0^\infty \int_0^\infty \frac{\tilde{r}_b^{U-2} e^{-\frac{r_b + \tilde{r}_b}{2}}}{2^U \Gamma(U-1)} [G(\gamma; r_b, \tilde{r}_b)]^{L_b} dr_b d\tilde{r}_b, \quad (29)$$

with  $G(\gamma; r_b, \tilde{r}_b)$  given by (30) (at the top of next page), where  $Q_p(\cdot, \cdot)$  is the  $p$ -th order Marcum-Q function and  $I_\nu(\cdot)$  is the  $\nu$ -th order modified Bessel function of the first kind.

*Proof:* See Appendix B. ■

Note that each product term in (29), representing the contribution of each block in (18), has exactly the same form as [8, Eq. (21)]; this guarantees the same analytical tractability, as compared with the oversimplified constant correlation model of [8]. To alleviate the computational effort of evaluating several double-integrals, Gauss-Laguerre quadrature can be used, leading to

$$\hat{P}_{\text{out}}(\gamma) \approx \prod_{b=1}^B \frac{1}{\Gamma(U-1)} \sum_{m=1}^M \sum_{\tilde{m}=1}^{\tilde{M}} w_m \tilde{w}_{\tilde{m}} [G(\gamma; 2x_m, 2\tilde{x}_{\tilde{m}})]^{L_b}, \quad (31)$$

where  $x_m$  for  $m = 1, \dots, M$  and  $\tilde{x}_{\tilde{m}}$  for  $\tilde{m} = 1, \dots, \tilde{M}$  are, respectively, the roots of the Laguerre polynomials  $L_M(x)$  and  $L_{\tilde{M}}^{U-2}(x)$ , and

$$w_m = \frac{x_m}{(M+1)^2 [L_{M+1}(x_m)]}, \quad (32)$$

$$\tilde{w}_{\tilde{m}} = \frac{\Gamma(\tilde{M} + U - 1) \tilde{x}_{\tilde{m}}}{\tilde{M}! (\tilde{M} + 1)^2 [L_{\tilde{M}+1}^{U-2}(\tilde{x}_{\tilde{m}})]}. \quad (33)$$

Equation (31) considerably reduces the computational effort, since the function  $G(\cdot)$  needs to be computed only once for each pair  $(x_m, \tilde{x}_{\tilde{m}})$ , regardless of the number of blocks  $B$ .

Interestingly, a further approximation to (29) can be obtained by particularizing for  $\mu \rightarrow 1$ , which is a requisite for the proposed block-diagonal approximation in Section III-B.

To that end, first notice that the sum in (30) is dominated by the exponential term as  $\mu \rightarrow 1$  and can thus be neglected, leading to

$$[G(\gamma; r_b, \tilde{r}_b)]^{L_b} \approx \left[ Q_{U-1} \left( \sqrt{\frac{\mu^2 \gamma \tilde{r}_b}{(1-\mu^2)(\gamma+1)}}, \sqrt{\frac{\mu^2 r_b}{(1-\mu^2)(\gamma+1)}} \right) \right]^{L_b}. \quad (34)$$

Besides, the spectral analysis in Section III-A highlights that, for very large  $N$ , only a very small fraction of eigenvalues is relevant. This implies that  $B \ll N$ , and since  $\sum_b^B L_b = N$ , we can expect very large values for each  $L_b$  (at least for most of the dominant eigenvalues). A large exponent strengthens the sigmoid behaviour of  $Q_p(\cdot)$ , and in the limit ( $L_b \rightarrow \infty$ )  $(Q_p(\cdot))^{L_b}$  becomes a simple step function. We propose to introduce this approximation in (29), as stated in the following corollary:

*Corollary 3:* For  $\mu \rightarrow 1$ , the outage probability for the block-diagonal correlation model is approximated by

$$\hat{P}_{\text{out}}(\gamma) \approx \prod_{b=1}^B \left[ 1 - \frac{2^{1-U}}{\Gamma(U-1)} \int_0^\infty \tilde{r}_b^{U-2} e^{(-\tilde{r}_b - \delta(\tilde{r}_b))/2} d\tilde{r}_b \right], \quad (35)$$

where  $\delta(\tilde{r}_b)$  is given by

$$\delta(\tilde{r}_b) = \left( \sqrt{\gamma \tilde{r}_b} + \frac{\frac{(U-\frac{3}{2})(1+\gamma)^{\frac{1}{2}}}{\mu(1-\mu^2)^{-\frac{1}{2}}} - \frac{L-1}{\sqrt{2\pi}} \sqrt{\gamma \tilde{r}_b}}{\frac{(L-1)(U-\frac{3}{2})}{\sqrt{2\pi}} + \sqrt{\frac{\mu^2 \gamma \tilde{r}_b}{(1-\mu^2)(1+\gamma)}}} \right)^2. \quad (36)$$

*Proof:* See Appendix C. ■

Again, Gauss-Laguerre quadrature can be applied to (35), leading to

$$\hat{P}_{\text{out}}(\gamma) \approx \prod_{b=1}^B \left[ 1 - \frac{1}{\Gamma(U-1)} \sum_{\tilde{m}} \tilde{w}_{\tilde{m}} e^{-\frac{1}{2}\delta(2\tilde{x}_{\tilde{m}})} \right], \quad (37)$$

where  $\tilde{w}_{\tilde{m}}$  and  $\tilde{x}_{\tilde{m}}$  are as in (31), improving the computational efficiency.

Corollary 3 provides a much simpler expression for the outage probability, with the accuracy of the approximation given (to some extent) by the choice of  $\delta(\tilde{r}_b)$ . The threshold in (36) is selected such that  $[G(\gamma; r_b, \tilde{r}_b)]^{L_b} \approx \frac{1}{2}$ , corresponding to the point of steepest slope. Interestingly enough, (35) allows to arbitrarily choose  $\delta(\tilde{r}_b)$  so that different upper and lower bounds are obtained. For instance, for an arbitrary Marcum's function  $Q_p(\alpha, z)$ , it is known that  $Q_p(\infty, z) = 1$  while  $Q_p(\alpha, \infty) = 0$ . When both  $\alpha$  and  $z$  grow rapidly, as in (34) due to the term  $1 - \mu$  in the denominators, the trivial choice  $z = \alpha$  as threshold value is motivated. Comparing with (34), this yields  $\delta(\tilde{r}_b) = \gamma \tilde{r}_b$ , which introduced in (35) leads to

$$\hat{P}_{\text{out}}^{\text{iid}}(\gamma) \approx \left( 1 - \frac{1}{(\gamma+1)^{U-1}} \right)^B, \quad (38)$$

where [32, Eq. (3.351 3)] has been used. Remarkably, the above expression is exactly the outage probability obtained by  $B$  independent antennas, as proved in Appendix D. Hence, the block-diagonal correlation model analytically connects with the heuristic approximation taken in Section III-C. Relating

$$G(\gamma; r_b, \tilde{r}_b) = Q_{U-1} \left( \sqrt{\frac{\mu^2 \gamma \tilde{r}_b}{(1-\mu^2)(\gamma+1)}}, \sqrt{\frac{\mu^2 r_b}{(1-\mu^2)(\gamma+1)}} \right) - \left( \frac{1}{\gamma+1} \right)^{U-1} \exp \left( -\frac{\mu^2}{2(1-\mu^2)} \frac{\gamma \tilde{r}_b + r_b}{\gamma+1} \right) \\ \times \sum_{k=0}^{U-2} \sum_{j=0}^{U-k-2} \frac{(U-(j+k)-1)_j}{j!} \left( \frac{r_b}{\tilde{r}_b} \right)^{\frac{j+k}{2}} (\gamma+1)^k \gamma^{\frac{j-k}{2}} I_{j+k} \left( \frac{\mu^2 \sqrt{\gamma r_b \tilde{r}_b}}{(1-\mu^2)(\gamma+1)} \right). \quad (30)$$

(38) to (35), we can obtain the approximated gain, in terms of outage probability, obtained by oversampling the fluid antenna—i.e., the gain rendered by going from a single antenna to a block of correlated elements. Specifically, defining by  $\Delta P_{\text{out}}^b$  the difference in outage probability achieved by the  $b$ -th block in (38) and (35), we have that

$$\Delta P_{\text{out}}^b = \frac{2^{1-U}}{\Gamma(U-1)} \int_0^\infty \tilde{r}_b^{U-2} e^{(-\tilde{r}_b - \delta(\tilde{r}_b))/2} d\tilde{r}_b - \frac{1}{(\gamma+1)^{U-1}}, \quad (39)$$

and, therefore,

$$\hat{P}_{\text{out}}(\gamma) = \prod_{b=1}^B \left[ 1 - \frac{1}{(\gamma+1)^{U-1}} - \Delta P_{\text{out}}^b \right]. \quad (40)$$

As example, the gain  $\Delta P_{\text{out}}^b$  for an arbitrary block is depicted in Fig. 6 for different number of users  $U$ , block sizes  $L$  and thresholds  $\gamma$ . Interestingly, we observe the expected saturation effect as  $L$  increases, since a large block size means that the ratio  $N/W$  is large and, hence, a dense fluid antenna. Besides, the gain rendered by the oversampling achieved by FAS is less noticeable as the number of users increases, due to the higher interference, and as the threshold  $\gamma$  is increased. Note also that this is a per-block gain, and therefore stacks with the gains achieved by the other blocks in (35). Thus, the larger the number of blocks, the more the benefit we can obtain from the large available number of ports. More ports means a larger fluid antenna (since we have, approximately, one block per half-wavelength), pointing out that the benefit of FAS is more evident as large apertures are available.  $\Delta P_{\text{out}}^b$  arises then as a useful expression to understand the benefit yielded by FAS.

## V. NUMERICAL RESULTS: PERFORMANCE EVALUATION OF SLOW-FAMA

The purpose of this section is twofold: first, we aim to evaluate the accuracy of the proposed approximation framework for spatial correlation in FAS; second, we target the performance evaluation of slow-FAMA systems. Specifically, we are interested in *i*) the impact of the fluid antenna size, *ii*) the saturation effect as the number of ports increases, *iii*) the number of simultaneous users supported by the system, and *iv*) whether the approximated expressions can capture all these effects. For the ease of presentation, we split the results into one-dimensional and two-dimensional FAS.

### A. One-dimensional FAS

Without loss of generality, we consider a linear fluid antenna along the  $x$  axis of length  $W$  (normalized by the wavelength)

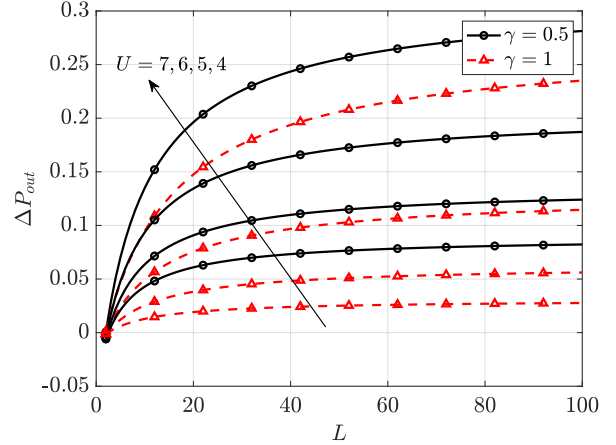


Fig. 6. Gain, in terms of outage probability, achieved by each block of correlated elements ( $\mu^2 = 0.97$ ) in (35) w.r.t. a single antenna element.

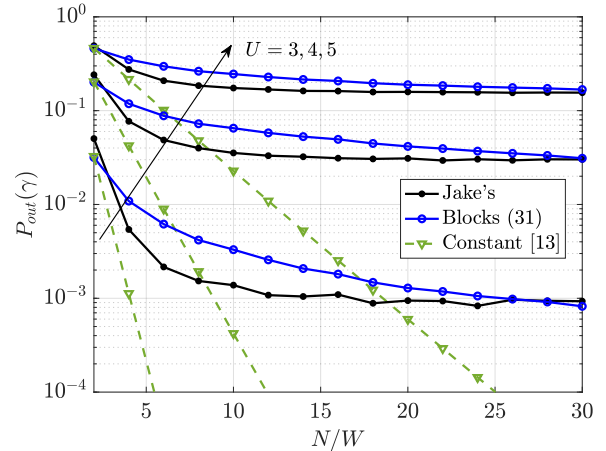


Fig. 7. Evolution of outage probability as the fluid antenna is densified. Jake's model (9) is compared with the proposed approximation and the model in [13]. Parameters:  $W = 6$ ,  $\gamma = 1$ ,  $\mu^2 = 0.97$ ,  $\rho_{\text{th}} = N/100$ .

and  $N$  equally spaced ports. Unless otherwise stated, the proposed approximations (29) and (35), resulting from applying Algorithm 1, are evaluated through the quadrature expressions in (31) and (37), respectively, with  $M = \bar{M} = 30$ .

With this setup, we first evaluate in Fig. 7 the outage probability achieved by slow-FAMA as  $N$  increases for different numbers of users. Jake's correlation (9) is assumed, and the constant correlation model in [13] is also plotted as baseline. As expected, for fixed  $W$ , densifying the fluid aperture leads to diminishing returns, saturating the system. This effect is also reported in [5, 6]. Specifically, more than 15 ports per

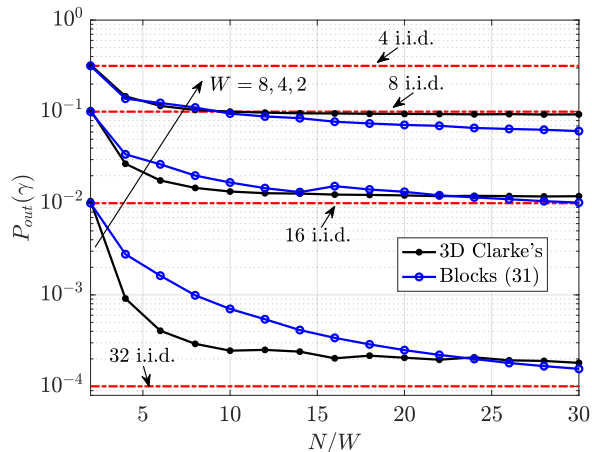


Fig. 8. Evolution of outage probability as the fluid antenna is densified. 3D Clarke's model (7) is compared with the proposed approximation. Parameters:  $U = 3$ ,  $\gamma = 1$ ,  $\mu^2 = 0.97$ ,  $\rho_{th} = N/100$ .

wavelength ( $N/W = 15$ ) seems to provide no additional benefit due to the already large correlation between adjacent ports. Relating it to Section III-A, the resulting correlation matrix no longer increases its rank significantly from this threshold point. Interestingly, we observe that the proposed block-diagonal approximation can capture this saturation, while the constant correlation model considerably deviates from the real performance (Jake's correlation simulation). The same trend is observed for Clarke's model in (11) and for different fluid antenna sizes, as illustrated in Fig. 8. This figure also depicts the performance achieved by a collection of independent antennas, given by (38). Note that, given a linear fluid antenna of length  $W$ , only  $2W$  independent antennas (equivalently,  $N/W = 2$ ) could be embedded in the same physical aperture, given that the  $\lambda/2$  spacing rule-of-thumb is followed. Hence, the gain of FAS is noticeable by just adding a few extra ports per wavelength. We also observe that, the larger the fluid antenna, the more the gain obtained w.r.t. the independent antenna system, as predicted by the stacking of the gains in (39). As a remark, it can be seen in both figures that, as the fluid antenna is densified, the accuracy of the proposed approximation increases. This is a coherent result, since the block-diagonal approximation arises from the asymptotic matrix results in Section III-A, being therefore a reasonable solution to analyze the limit performance of FAS.

Looking at the left tail of  $P_{out}(\gamma)$ , Fig. 9 depicts the outage probability under Jake's correlation for different number of users. On top of the ground-truth simulated curve, it also shows the one obtained by the block-diagonal approximation (31), its approximated expression for large  $\mu$  (37) with the threshold value in (36), the upper bound in (38) and the result achieved by the constant correlation model in [13]. As before, we observe that the constant correlation model is overly too optimistic, while both approximated expressions arising from the block-diagonal framework are tight. The upper bound based on independent antennas is naturally pessimistic, since it assumes perfect correlation within each block; its usefulness is though given by its simplicity and its ability to somehow

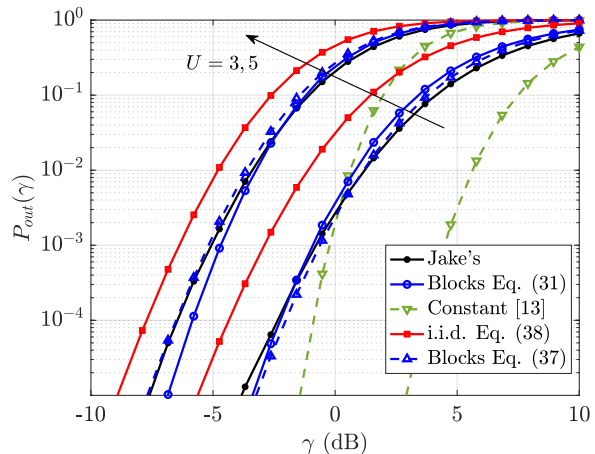


Fig. 9. Outage probability in terms of  $\gamma$ . Jake's model is compared with the proposed approximation, the i.i.d. upper bound, and the constant correlation model in [13]. Parameters:  $N = 100$ ,  $W = 5$ ,  $\mu^2 = 0.97$ ,  $\rho_{th} = N/100$ .

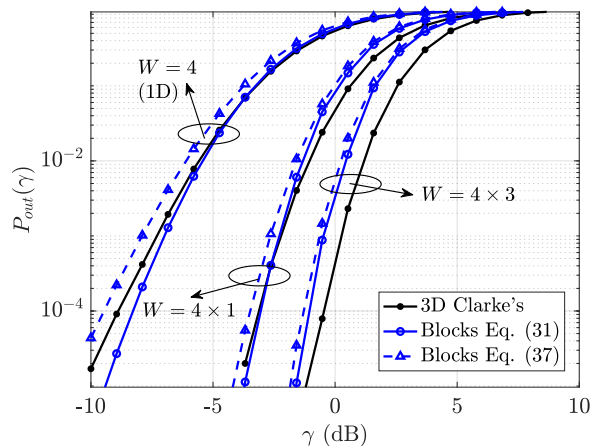


Fig. 10. Outage probability in terms of  $\gamma$  for different fluid antenna size. 3D Clarke's (7) model is compared with the proposed approximation. Parameters: 15 ports per wavelength,  $U = 6$ ,  $\mu^2 = 0.97$ ,  $\rho_{th} = 1$ .

capture the general trend of the system (as opposite to the constant correlation model).

## B. Two-dimensional FAS

Moving on to 2D FAS, consider now a planar fluid antenna of area  $W = W_x \times W_z$  contained in the  $xz$ -plane, where both  $W_x$  and  $W_z$  are normalized by the wavelength. The total number of ports is  $N = N_x \times N_z$ , being again equally spaced along both axes. Since Jake's correlation is not valid for these planar apertures, we here stick to 3D Clarke's model (11).

Motivated by the promising results reported in [9] on two-dimensional FAS, we first evaluate in Fig. 10 the gain—in terms of outage probability—achieved by going from 1D to 2D fluid antennas. Interestingly, the gap between a linear antenna of size  $W = 4$  and a 2D antenna of size  $W = 4 \times 1$  is quite significant, suggesting that even a thin—albeit planar—surface may be more interesting than large and linear apertures in terms of performance. On the other hand, the accuracy of the

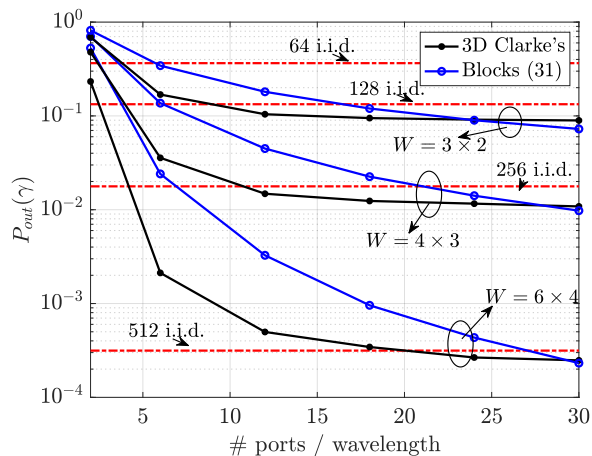


Fig. 11. Evolution of outage probability as the 2D fluid aperture is densified. 3D Clarke's model (7) is compared with the proposed approximation. Parameters:  $U = 7$ ,  $\gamma = 1$ ,  $\mu^2 = 0.96$ ,  $\rho_{th} = 1$ .

proposed approximation (both (29) and (35)) is high regardless the fluid antenna size.

As in Fig. 8, the saturation effect and the performance comparison with independent antenna systems are now evaluated for 2D FAS in Fig. 11, where similar conclusions are drawn. First, we observe how the system gain saturates after a certain number of ports per wavelength, albeit the 2D aperture seem to benefit from a denser mesh of ports as compared with linear apertures; recall that in the 1D case, 10 to 15 ports per wavelength was enough to notice the saturation effect. Second, the performance gap w.r.t. the independent antenna system is larger as the fluid antenna size increases, in agreement with the analysis of Section IV-B. Last, we also see that the approximated expression in (31) gets tighter as the fluid antenna is densified.

Finally, Fig. 12 evaluates the outage probability of slow-FAMA as the number of users increases. Interestingly, a quick saturation of the system can be observed as the number of users grows. Naturally, larger fluid antennas support a larger number of users, but the performance rapidly drops as more users are added. It is important to remember, though, that no precoding nor interference cancellation techniques are used, so the multiplexing capacity is still relevant. We also observe that the block approximation in (29) is once again tight regardless of the system parameters, although the simplified expression in (35) deviates from the ground-truth performance for some particular settings.

## VI. CONCLUSIONS

The proposed spatial block-correlation model has been shown to be an interesting workaround to alleviate the high analytical complexity inherent to realistic spatial correlation models such as Clarke's or Jake's. The use of block-diagonal correlation matrices to characterize FAS is well supported by asymptotic results on large Toeplitz—thus, correlation—matrices, and can approximate the performance of slow-FAMA systems tightly without penalizing the tractability of other state-of-the-art (oversimplified) models that fail in predicting

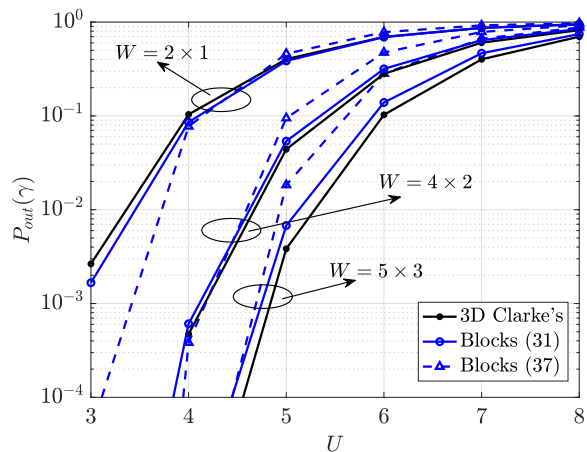


Fig. 12. Evolution of outage probability for different number of simultaneous users. 3D Clarke's model (7) is compared with the proposed approximation. Parameters: 20 ports per wavelength,  $\gamma = 2$ ,  $\mu^2 = 0.95$ ,  $\rho_{th} = 1$ .

realistic results. Although the hyperparameters of the model (namely, correlation within each block and number of blocks) have been chosen somewhat heuristically, this paper proves the potential of the block-correlation approximation and its versatility to fit any arbitrary correlation structure of the wireless channel. Hence, the proposed framework arises as a tool to fully answer fundamental questions inherent to FAS, such as the performance gain obtained by the dense oversampling of the fluid aperture.

The fact that a completely different correlation structure successfully captures the performance achieved by realistic (physics-based) correlation models also points out that further studies are necessary to fully understand the impact of spatial correlation in FAS. Understanding the performance limits of FAS is still necessary before facing other challenges such as its integration with other technologies and practical physical implementations, and given the high complexity inherent to spatial correlation models, alternative tools such as the proposed framework may become feasible solutions and interesting pathways to explore.

## APPENDIX A

### EIGENVALUES OF BLOCK-DIAGONAL MATRICES

Given the matrix structure in (18), the eigenvalues of  $\hat{\Sigma}$  are those of  $\mathbf{A}_1, \dots, \mathbf{A}_B$ . The eigenvalues of each block  $\mathbf{A}_b$  are obtained as the solutions to

$$|\mathbf{A}_b - \rho \mathbf{I}| = \begin{vmatrix} 1 - \rho & \mu_b^2 & \cdots & \mu_b^2 \\ \mu_b^2 & 1 - \rho & \cdots & \mu_b^2 \\ \vdots & & \ddots & \vdots \\ \mu_b^2 & \cdots & \mu_b^2 & 1 - \rho \end{vmatrix} = 0. \quad (41)$$

Since the determinant is invariant to linear rows/columns combinations, we successively subtract to each row the one immediately below, leading to

$$\begin{vmatrix} 1 - \rho - \mu_b^2 & \mu_b^2 + \rho - 1 & 0 & \cdots & 0 \\ 0 & 1 - \rho - \mu_b^2 & \mu_b^2 + \rho - 1 & \cdots & 0 \\ \vdots & & & \ddots & \vdots \\ \mu_b^2 & \mu_b^2 & \cdots & \mu_b^2 & 1 - \rho \end{vmatrix} = 0. \quad (42)$$

Similarly, we now add to each column the one immediately to the left, yielding

$$\left| \begin{pmatrix} 1-\rho-\mu_b^2 & 0 & 0 & \cdots & 0 \\ 0 & 1-\rho-\mu_b^2 & 0 & \cdots & 0 \\ \vdots & \vdots & \vdots & \ddots & \vdots \\ \mu_b^2 & 2\mu_b^2 & \cdots & (L_b-1)\mu_b^2 & 1-\rho+(L_b-1)\mu_b^2 \end{pmatrix} \right| = 0. \quad (43)$$

Hence, each block  $\mathbf{A}_b$  renders a simple eigenvalue  $\rho = (L_b - 1)\mu_b^2 + 1$  and a multiple eigenvalue  $\rho = 1 - \mu_b^2$  with multiplicity  $L_b - 1$ .

#### APPENDIX B PROOF OF LEMMA 2

The outage probability in (29) is obtained by following similar steps as in [8, Appendix B] to each block of the approximated correlation matrix. The superscripts  $(\tilde{u}, u)$  and  $(u, u)$  are omitted for ease of notation.

##### A. Joint PDF and CDF of $\{X_n\}$

Conditioned on  $r_b \triangleq x_b^2 + y_b^2 \forall b$ ,  $X_n$  is a non-central Chi-square random variable with two degrees of freedom—equivalently, a squared Rician random variable—with probability density function (PDF)

$$f_{X_n|r_b}(x) = \frac{1}{2} \exp\left(-\frac{x + \frac{\mu^2}{1-\mu^2}r_b}{2}\right) I_0\left(\sqrt{\frac{\mu^2 r_b x}{1-\mu^2}}\right). \quad (44)$$

Since the variables in  $\{X_n\}$  are all linked by  $\{r_b\}$ , then they are conditionally independent with PDF

$$f_{\{X_n\}|\{r_b\}}(x_1, \dots, x_N) = \prod_{b=1}^B \prod_{n \in \mathcal{N}_b} \frac{1}{2} \exp\left(-\frac{x_n + \frac{\mu^2}{1-\mu^2}r_b}{2}\right) \times I_0\left(\sqrt{\frac{\mu^2 r_b x_n}{1-\mu^2}}\right). \quad (45)$$

In (45), to clearly highlight the block correlation model, we have specifically split the product into the different blocks and the  $n$  indices within each block. Hence,  $\mathcal{N}_b$  denotes the set of  $n$  indices corresponding to block  $b$  (note that  $|\mathcal{N}_b| = L_b$ ). To obtain the unconditioned joint PDF, (45) is averaged over the distribution of  $r_b$ 's, which are independent and follow exponential distributions with PDF

$$f_{r_b}(r_b) = \frac{1}{2} e^{-r_b/2}, \quad b = 1, \dots, B, \quad (46)$$

leading to

$$\begin{aligned} f_{\{X_n\}}(x_1, \dots, x_N) &= \int_0^\infty \cdots \int_0^\infty f_{\{X_n\}|\{r_b\}}(x_1, \dots, x_N) \\ &\times \prod_{b=1}^B f_{r_b}(r_b) dr_1 \cdots dr_B \\ &= \prod_{b=1}^B \int_0^\infty \frac{1}{2^{L_b+1}} e^{-r_b/2} \prod_{k \in \mathcal{K}_b} \exp\left(-\frac{x_k + \frac{\mu_b^2}{1-\mu_b^2}r_b}{2}\right) \\ &\times I_0\left(\sqrt{\frac{\mu_b^2 r_b x_k}{1-\mu_b^2}}\right) dr_b. \end{aligned} \quad (47)$$

The joint cumulative distribution function (CDF) is obtained from (47) as

$$\begin{aligned} F_{\{X_n\}}(t_1, \dots, t_N) &= \int_0^{t_1} \cdots \int_0^{t_N} f_{\{X_n\}}(\cdot) dx_1 \cdots dx_N \\ &\stackrel{(a)}{=} \prod_{b=1}^B \int_0^\infty \frac{1}{2} e^{-r_b/2} \prod_{n \in \mathcal{N}_b} \left[1 - Q_1\left(\sqrt{\frac{\mu^2 r_b}{1-\mu^2}}, \sqrt{t_n}\right)\right] dr_b, \end{aligned} \quad (48)$$

where the CDF of the Rician distribution is identified in (a).

##### B. Joint PDF of $\{Y_n\}$

The joint PDF of  $\{Y_n\}$  is obtained by following the same steps as in the case of  $\{X_n\}$ . First, conditioned on  $\tilde{r}_b \triangleq \sum_{\tilde{u} \neq u} (x_b^{\tilde{u}, u})^2 + (y_b^{\tilde{u}, u})^2$  for  $b = 1, \dots, B$ ,  $Y_n$  is non-central  $\chi^2$  distributed with  $2(U - 1)$  degrees of freedom and PDF

$$\begin{aligned} f_{Y_n|\tilde{r}_b}(y) &= \frac{1}{2} \left(\frac{y(1-\mu^2)}{\mu^2 \tilde{r}_b}\right)^{\frac{U-2}{2}} \exp\left(-\frac{y + \frac{\mu^2}{1-\mu^2} \tilde{r}_b}{2}\right) \\ &\times I_{U-2}\left(\sqrt{\frac{\mu^2 \tilde{r}_b y}{1-\mu^2}}\right). \end{aligned} \quad (49)$$

Finally, averaging over the set  $\{\tilde{r}_b\}$  (each of which is central  $\chi^2$  distributed), the joint PDF of  $\{Y_n\}$  is given by

$$\begin{aligned} f_{\{Y_n\}}(y_1, \dots, y_N) &= \prod_{b=1}^B \int_0^\infty \frac{\tilde{r}_b^{U-2} e^{-\tilde{r}_b/2}}{2^{U-1} \Gamma(U-1)} \\ &\times \prod_{n \in \mathcal{N}_b} \frac{1}{2} \left(\frac{y_n(1-\mu^2)}{\mu^2 \tilde{r}_b}\right)^{\frac{U-2}{2}} \exp\left(-\frac{y_n + \frac{\mu^2}{1-\mu^2} \tilde{r}_b}{2}\right) \\ &\times I_{U-2}\left(\sqrt{\frac{\mu^2 \tilde{r}_b y_n}{1-\mu^2}}\right) d\tilde{r}_b. \end{aligned} \quad (50)$$

##### C. Outage probability

From (26), the outage probability is obtained as

$$\begin{aligned} \hat{P}_{\text{out}}(\gamma) &= P\left(\frac{X_1}{Y_1} < \gamma, \dots, \frac{X_N}{Y_N} < \gamma\right) \\ &= \int_0^\infty \cdots \int_0^\infty F_{\{X_n\}|\{Y_n\}}(\gamma y_1, \dots, \gamma y_N) \\ &\times f_{\{Y_n\}}(y_1, \dots, y_N) dy_1 \cdots dy_N. \end{aligned} \quad (51)$$

Introducing (48) and (50) leads to (52) at the top of next page, from which (29) is obtained by using the results from [8, Corollary 1].

#### APPENDIX C PROOF OF COROLLARY 3

Consider first  $\delta(\tilde{r}_b)$  as an arbitrary threshold such that  $[G(\gamma; r_b, \tilde{r}_b)]^{L_b} = 1$  for  $r_b < \delta(\tilde{r}_b)$  and  $[G(\gamma; r_b, \tilde{r}_b)]^{L_b} = 0$  for  $r_b > \delta(\tilde{r}_b)$ . Then, for large  $L_b$ ,  $[G(\gamma; r_b, \tilde{r}_b)]^{L_b}$  in (34)

$$\begin{aligned}
\widehat{P}_{\text{out}}(\gamma) &= \underbrace{\int_0^\infty \cdots \int_0^\infty}_{y_1, \dots, y_N} \prod_{b=1}^B \int_0^\infty \int_0^\infty \frac{\widetilde{r}_b^{U-2} e^{-\frac{r_b + \widetilde{r}_b}{2}}}{2^U \Gamma(U-1)} \prod_{n \in \mathcal{N}_b} \frac{1}{2} \left[ 1 - Q_1 \left( \sqrt{\frac{\mu^2 r_b}{1-\mu^2}}, \sqrt{\gamma y_n} \right) \right] \left( \frac{y_n (1-\mu^2)}{\mu^2 \widetilde{r}_b} \right)^{\frac{U-2}{2}} \\
&\quad \times \exp \left( -\frac{y_n + \frac{\mu^2}{1-\mu^2} \widetilde{r}_b}{2} \right) I_{U-2} \left( \sqrt{\frac{\mu^2 \widetilde{r}_b y_n}{1-\mu^2}} \right) dr_b d\widetilde{r}_b dy_1 \cdots dy_N \\
&= \prod_{b=1}^B \int_0^\infty \int_0^\infty \frac{\widetilde{r}_b^{U-2} e^{-\frac{r_b + \widetilde{r}_b}{2}}}{2^U \Gamma(U-1)} \prod_{n \in \mathcal{N}_b} \left[ 1 - \frac{1}{2} \int_{y_n=0}^\infty Q_1 \left( \sqrt{\frac{\mu^2 r_b}{1-\mu^2}}, \sqrt{\gamma y_n} \right) \left( \frac{y_n (1-\mu^2)}{\mu^2 \widetilde{r}_b} \right)^{\frac{U-2}{2}} \right. \\
&\quad \left. \times \exp \left( -\frac{y_n + \frac{\mu^2}{1-\mu^2} \widetilde{r}_b}{2} \right) I_{U-2} \left( \sqrt{\frac{\mu^2 \widetilde{r}_b y_n}{1-\mu^2}} \right) \right] dr_b d\widetilde{r}_b. \tag{52}
\end{aligned}$$

can be approximated by the Heaviside step function shifted at  $\delta(\widetilde{r}_b)$  and, consequently, (29) is approximated by

$$\widehat{P}_{\text{out}}(\gamma) \approx \prod_{b=1}^B \int_0^\infty \frac{\widetilde{r}_b^{U-2} e^{-\widetilde{r}_b/2}}{2^U \Gamma(U-1)} \int_0^{\delta(\widetilde{r}_b)} e^{-r_b/2} dr_b d\widetilde{r}_b, \tag{53}$$

Solving the inner integral and using [32, Eq. (3.351 3)], (35) is obtained.

The remaining step is calculating  $\delta(\widetilde{r}_b)$ . Since  $[Q_p(\cdot)]^L$  corresponds to the product of the complementary CDFs of  $L_b$  i.i.d. non-central  $\chi^2$  variables, a reasonable choice for the threshold  $\delta(\widetilde{r}_b)$  can be obtained by seeking the value of  $r_b$  for which  $[G(\gamma; r_b, \widetilde{r}_b)]^{L_b} = \frac{1}{2}$ . This value corresponds to the point of steepest slope, i.e., the minimum of the derivative (since  $Q_p(\cdot)$  is monotonically decreasing) [33]. Thus, we aim to solve

$$\arg \min_z \frac{\partial [Q_p(\alpha, z)]^L}{\partial z}. \tag{54}$$

The partial derivative w.r.t.  $z$  is given by

$$\begin{aligned}
\frac{\partial [Q_p(\alpha, z)]^L}{\partial z} &= -L [Q_p(\alpha, z)]^{L-1} \frac{z^p}{\alpha^{p-1}} e^{-\frac{\alpha^2 + z^2}{2}} I_{p-1}(\alpha z) \\
&\stackrel{(a)}{\approx} -\frac{L}{\sqrt{2\pi}} [Q_p(\alpha, z)]^{L-1} \frac{z^{p-\frac{1}{2}}}{\alpha^{p-\frac{1}{2}}} e^{-\frac{(\alpha-z)^2}{2}}, \tag{55}
\end{aligned}$$

where, in (a), the first term of the asymptotic expansion in [34, Eq. (9.7.1)] for the Bessel's function is applied. Equating the partial w.r.t.  $z$  of (55) to zero, and applying again the first term of the expansion for  $I_\nu(\cdot)$ , we obtain

$$\begin{aligned}
&-\frac{(L-1)}{\sqrt{2\pi}} [Q_p(\alpha, z)]^{L-2} \frac{z^{p-\frac{1}{2}}}{\alpha^{p-\frac{1}{2}}} e^{-\frac{(\alpha-z)^2}{2}} \\
&+ [Q_p(\alpha, z)]^{L-1} \frac{p-\frac{1}{2}}{z} + [Q_p(\alpha, z)]^{L-1} (\alpha-z) = 0. \tag{56}
\end{aligned}$$

For large  $L$ ,  $[Q_p(\alpha, z)]^{L-1} \approx [Q_p(\alpha, z)]^{L-2}$  due to the sigmoid behaviour of  $Q_p(\cdot)$ , leading to

$$-\frac{(L-1)}{\sqrt{2\pi}} \frac{z^{p-\frac{1}{2}}}{\alpha^{p-\frac{1}{2}}} e^{-\frac{(\alpha-z)^2}{2}} + \frac{p-\frac{1}{2}}{z} + \alpha - z = 0, \tag{57}$$

where the sought value of  $z$  is the solution to the above equation. To obtain an approximated closed-form solution,

the first order Taylor's series can be taken around the point  $z = \alpha$ . This choice is justified as follows: if  $z < \alpha$ , then  $Q_p(\alpha, z) \rightarrow 1$ , while  $Q_p(\alpha, z) \rightarrow 0$  given  $z > \alpha$ ; therefore, it is reasonable to assume that the solution to (57) is in a relatively small neighbourhood around  $\alpha$ . Therefore, we get

$$z \approx \alpha - \frac{-\frac{(L-1)}{\sqrt{2\pi}} + \alpha^{-1}(p-\frac{1}{2})}{-\frac{L-1}{\sqrt{2\pi}}(p-\frac{1}{2})\alpha^{-1} - \alpha^{-2}(p-\frac{1}{2}) - 1} \tag{58}$$

which, under the assumption of  $\alpha \gg p$ , yields

$$z \approx \alpha + \frac{p-\frac{1}{2} - \alpha \frac{L-1}{\sqrt{2\pi}}}{\frac{L-1}{\sqrt{2\pi}}(p-\frac{1}{2}) + \alpha}. \tag{59}$$

Comparing (59) with (34) finally leads to (36), completing the proof.

## APPENDIX D

### OUTAGE PROBABILITY OF I.I.D. ANTENNAS

Considering  $B$  independent antennas, the involved variables in (26) are given by

$$X_n = \left( x_n^{(u,u)} \right)^2 + \left( y_n^{(u,u)} \right)^2, \tag{60}$$

$$Y_n = \sum_{\widetilde{u}=1, \widetilde{u} \neq u}^U \left( x_n^{(\widetilde{u},u)} \right)^2 + \left( y_n^{(\widetilde{u},u)} \right)^2, \tag{61}$$

where all the involved variables are independent zero-mean Gaussian variables with unit variance. Therefore,  $X_n$  is exponentially distributed with joint CDF

$$F_{\{X_n\}}(t_1, \dots, t_B) = \prod_{n=1}^B 1 - e^{-t_n/2}. \tag{62}$$

Similarly,  $Y_n$  is central  $\chi^2$  distributed with  $2(U-1)$  degrees of freedom with joint PDF

$$f_{\{Y_n\}}(y_1, \dots, y_B) = \prod_{n=1}^B \frac{1}{2^{U-1} \Gamma(U-1)} y_n^{U-2} e^{-y_n/2}. \tag{63}$$

The outage probability is then easily calculated as

$$\begin{aligned}
P_{\text{out}}(\gamma) &= \int_0^\infty \cdots \int_0^\infty F_{\{X_n\}|\{Y_n\}}(\gamma y_1, \dots, \gamma y_B) \\
&\quad \times f_{\{Y_n\}}(y_1, \dots, y_B) dy_1 \cdots dy_B, \tag{64}
\end{aligned}$$

which, after algebraic manipulations and the use of [32, Eq. (3.351 3)] yields (38).

## REFERENCES

- [1] K.-K. Wong, K.-F. Tong, Y. Shen, Y. Chen, and Y. Zhang, "Bruce lee-inspired fluid antenna system: Six research topics and the potentials for 6G," *Front. Comms. Net.*, vol. 3, 2022.
- [2] A. Grau Besoli and F. De Flaviis, "A multifunctional reconfigurable pixeled antenna using MEMS technology on printed circuit board," *IEEE Trans. Antennas Propag.*, vol. 59, no. 12, pp. 4413–4424, 2011.
- [3] B. Cetiner, H. Jafarkhani, J.-Y. Qian, H. J. Yoo, A. Grau, and F. De Flaviis, "Multifunctional reconfigurable MEMS integrated antennas for adaptive MIMO systems," *IEEE Commun. Mag.*, vol. 42, no. 12, pp. 62–70, 2004.
- [4] Y. Huang, L. Xing, C. Song, S. Wang, and F. Elhouni, "Liquid antennas: Past, present and future," *IEEE Open J. Antennas Propag.*, vol. 2, pp. 473–487, 2021.
- [5] L. Zhu, W. Ma, B. Ning, and R. Zhang, "Movable-antenna enhanced multiuser communication via antenna position optimization," *IEEE Trans. Wireless Commun. (Early Access)*, pp. 1–1, 2023.
- [6] M. Khammassi, A. Kammoun, and M.-S. Alouini, "A new analytical approximation of the fluid antenna system channel," *IEEE Trans. Wireless Commun. (Early Access)*, pp. 1–1, 2023.
- [7] K.-K. Wong and K.-F. Tong, "Fluid antenna multiple access," *IEEE Trans. Wireless Commun.*, vol. 21, no. 7, pp. 4801–4815, 2022.
- [8] K.-K. Wong, D. Morales-Jimenez, K.-F. Tong, and C.-B. Chae, "Slow fluid antenna multiple access," *IEEE Trans. Commun.*, vol. 71, no. 5, pp. 2831–2846, 2023.
- [9] W. K. New, K.-K. Wong, H. Xu, K.-F. Tong, and C.-B. Chae, "An information-theoretic characterization of MIMO-FAS: Optimization, diversity-multiplexing tradeoff and q-outage capacity," *IEEE Trans. Wireless Commun. (Early Access)*, pp. 1–1, 2023.
- [10] A. Pizzo, T. L. Marzetta, and L. Sanguinetti, "Spatially-stationary model for holographic mimo small-scale fading," *IEEE Journal on Selected Areas in Communications*, vol. 38, no. 9, pp. 1964–1979, 2020.
- [11] K.-K. Wong, A. Shojaefard, K.-F. Tong, and Y. Zhang, "Fluid antenna systems," *IEEE Trans. Wireless Commun.*, vol. 20, no. 3, pp. 1950–1962, 2021.
- [12] W. K. New, K.-K. Wong, H. Xu, K.-F. Tong, and C.-B. Chae, "Fluid antenna system: New insights on outage probability and diversity gain," *IEEE Trans. Wireless Commun.*, pp. 1–1, 2023.
- [13] K. K. Wong, K. F. Tong, Y. Chen, and Y. Zhang, "Closed-form expressions for spatial correlation parameters for performance analysis of fluid antenna systems," *Electronics Lett.*, vol. 58, no. 11, pp. 454–457, 2022.
- [14] B. Tang, H. Xu, K.-K. Wong, K.-F. Tong, Y. Zhang, and C.-B. Chae, "Fluid antenna enabling secret communications," *IEEE Commun. Lett.*, vol. 27, no. 6, pp. 1491–1495, 2023.
- [15] S. Zhang, J. Mao, Y. Hou, Y. Chen, K.-K. Wong, Q. Cui, and X. Tao, "Fast port selection using temporal and spatial correlation for fluid antenna systems," in *2023 IEEE Stat. Signal Process. Workshop (SSP)*, 2023, pp. 95–99.
- [16] C. Skouroumounis and I. Krikidis, "Fluid antenna with linear MMSE channel estimation for large-scale cellular networks," *IEEE Transactions on Communications*, vol. 71, no. 2, pp. 1112–1125, 2023.
- [17] C. Psomas, P. J. Smith, H. A. Suraweera, and I. Krikidis, "Continuous fluid antenna systems: Modeling and analysis," *IEEE Commun. Lett. (Early access)*, pp. 1–1, 2023.
- [18] W. C. Jakes and D. C. Cox, *Microwave Mobile Communications*. Wiley-IEEE Press, 1994.
- [19] J. D. Vega-Sánchez, A. E. López-Ramírez, L. Urquiza-Aguiar, and D. P. M. Osorio, "Novel expressions for the outage probability and diversity gains in fluid antenna system," *IEEE Wireless Commun. Lett. (Early Access)*, pp. 1–1, 2023.
- [20] L. Tlebaldiyeva, S. Arzykulov, K. M. Rabie, X. Li, and G. Nauryzbayev, "Outage performance of fluid antenna system (FAS)-aided terahertz communication networks," 2023.
- [21] H. Yang, K.-K. Wong, K.-F. Tong, Y. Zhang, and C.-B. Chae, "Performance analysis of slow fluid antenna multiple access in noisy channels using gauss-laguerre and gauss-hermite quadratures," *IEEE Commun. Lett.*, vol. 27, no. 7, pp. 1734–1738, 2023.
- [22] X. Lai, T. Wu, J. Yao, C. Pan, M. El-kashlan, and K.-K. Wong, "On performance of fluid antenna system using maximum ratio combining," *IEEE Commun. Lett. (Early Access)*, pp. 1–1, 2023.
- [23] J. D. Vega-Sánchez, L. Urquiza-Aguiar, M. C. P. Paredes, and D. P. M. Osorio, "A simple method for the performance analysis of fluid antenna systems under correlated Nakagami-m fading," *IEEE Wireless Commun. Lett. (Early Access)*, pp. 1–1, 2023.
- [24] E. Björnson and L. Sanguinetti, "Rayleigh fading modeling and channel hardening for reconfigurable intelligent surfaces," *IEEE Wireless Commun. Lett.*, vol. 10, no. 4, pp. 830–834, 2021.
- [25] R. H. Clarke, "A statistical theory of mobile-radio reception," *Bell Syst. Tech. J.*, vol. 47, no. 6, pp. 957–1000, 1968.
- [26] T. Aulin, "A modified model for the fading signal at a mobile radio channel," *IEEE Trans. Veh. Technol.*, vol. 28, no. 3, pp. 182–203, 1979.
- [27] A. Goldsmith, *Wireless Communications*. Cambridge University Press, 2005.
- [28] D. Tse and V. Pramod, *Fundamentals of Wireless Communication*. United Kingdom: Cambridge University Press, 2005.
- [29] N. C. Beaulieu and K. T. Hemachandra, "Novel simple representations for Gaussian class multivariate distributions with generalized correlation," *IEEE Trans. Inf. Theory*, vol. 57, no. 12, pp. 8072–8083, 2011.
- [30] E. E. Tyrtshnikov, "A unifying approach to some old and new theorems on distribution and clustering," *Linear Algebra Its Appl.*, vol. 232, pp. 1–43, 1996.
- [31] H. Bateman and B. M. Project, *Tables of Integral Transforms*. McGraw-Hill Book Company, 1954, vol. 1.
- [32] I. S. Gradshteyn and I. M. Ryzhik, *Table of integrals, series, and products*, 7th ed. Academic press, 2007.
- [33] H. Guo, B. Makki, M.-S. Alouini, and T. Svensson, "A semi-linear approximation of the first-order Marcum Q-function with application to predictor antenna systems," *IEEE Open J. Commun. Soc.*, vol. 2, pp. 273–286, 2021.
- [34] M. Abramowitz and I. A. Stegun, *Handbook of Mathematical Functions with Formulas, Graphs, and Mathematical Tables*. New York: Dover, 1964.